Interfacial and microstructural properties of $SrTiO_3$ thin films grown on Si(001) substrates

J. Q. He,[a] S. Regnery,[b] C. L. Jia,[c] Y. L. Qin, F. Fitsilis, P. Ehrhart, R. Waser, and K. Urban
Institut für Festkörperforschung, Forschungszentrum Jülich GmbH, D-52425 Jülich, Germany

R. H. Wang
Department of Physics, Wuhan University, Wuhan 430072, People's Republic of China

(Received 17 July 2002; accepted 26 September 2002)

The microstructure and interfaces of $SrTiO_3$ thin films directly deposited by metalorganic chemical vapor deposition on silicon (001) substrates were investigated by means of Bragg-diffraction contrast and high-resolution transmission electron microscopy. The observation of the plan-view specimens showed that the $SrTiO_3$ films are polycrystalline with randomly oriented grains. An amorphous layer was observed at the interfaces between the films and the substrates. The growth kinetics of this amorphous layer was investigated in detail. The thickness showed a rapid initial increase, which is much faster than the corresponding growth of amorphous SiO_2 in the absence of precursors, and apparently approaches saturation after a short time. The thickness of the interfacial layer increases with the oxygen partial pressure during deposition and a reduction to a value acceptable for gate-oxide applications has been achieved for the minimum pressure given by the oxygen content of the present precursors. However, this comes at the cost of a dramatic increase of the carbon content of the film. © *2002 American Institute of Physics.* [DOI: 10.1063/1.1522475]

I. INTRODUCTION

High dielectric constant perovskite thin films, such as $SrTiO_3$ (STO), have been proposed for a very broad application area, including capacitor dielectrics for future dynamic random access memories (DRAMs), embedded capacitors, tunable devices, as well as gate oxides for field effect transistors (FETs) or ferroelectric field effect transistors. For capacitor applications, i.e., metal-insulator-metal (MIM) structures, there is wide experience with growth on suitable electrodes like Pt, Ru, or RuO_2.[1] For gate-oxide applications, i.e., metal-insulator-semiconductor (MIS) structures, an ultrathin oxide layer should, however, be grown directly on Si without interfacial SiO_x layers, which reduce the capacitance of the layer stack.[2] These high-κ gate oxides are of current interest because the traditionally used SiO_2 gate dielectrics in metal-oxide-semiconductor (MOS) devices have to be reduced in thickness along with the continuous reduction of the device scale demanded for ultra-large-scale-integration (ULSI) circuits, and due to increased tunneling currents a fundamental scaling limit will soon be reached. Therefore, the gate oxide has to be replaced by a material with higher permittivity.[2] In replacing SiO_2 it remains a challenge to achieve the required properties for films directly grown on the silicon substrates. Especially difficult is the elimination of interfacial layers with Low-κ values and/or high interfacial trap densities. Amorphous metal oxides, like Al_2O_3, HfO_2, and ZrO_2, are considered to be the most promising near-term replacement. Such amorphous gate oxides or silicates (e.g., $HfSiO_x$, $ZrSiO_x$) yield κ values in the range of 8–20. For even higher κ-values crystalline materials, especially STO, are being considered as epitaxial layers and, in spite of the possible complications by grain boundaries, also in the form of polycrystalline films.

Given the lattice parameters of STO ($a=0.3905$ nm) and silicon ($a=0.543$ nm), epitaxy with a small lattice mismatch of 1.7% can be obtained when the STO unit cell is rotated around the common [001] axis by 45° with respect to the silicon unit cell. However, STO is thermodynamically not stable on Si (Ref. 3) and in order to avoid the formation of an interfacial SiO_x layer growth must be achieved through special reaction paths. Molecular beam epitaxy (MBE) allows the start of deposition at extremely low oxygen partial pressures and has been used for the investigation of the growth conditions of epitaxial films. Early MBE approaches used SrO buffer layers of typically 10 nm thickness and achieved good heteroepitaxial growth.[4–6] Starting with the work of McKee *et al.*,[7] direct deposition (with an interfacial layer of Sr silicate and Sr oxide of subatomic thickness) has been achieved recently by MBE techniques.[7–11] Pulsed laser deposition (PLD) has also been employed to grow heteroepitaxial STO films on Si substrates.[12–14] However, only rather thick layers on different buffer layers have been reported so far.

Polycrystalline films have been deposited using more production-type tools. rf magnetron sputtering using Ar–oxygen mixtures as sputter gases yielded polycrystalline or partially oriented films due to the formation of interfacial layers.[15–17] Similarly, metalorganic chemical vapor deposi-

[a]Also at: Department of Physics, Wuhan University, Wuhan 430072, People's Republic of China.
[b]Also at: Aixtron AG, Kackertstr. 15-17, D-52072 Aachen, Germany.
[c]Author to whom correspondence should be addressed; electronic mail: c.jia@fz-juelich.de

tion (MOCVD) generally cannot reach ultralow oxygen partial pressures, and SiO_x interfacial layers yielding a polycrystalline growth[18–21] are formed if no additional stable buffer layers are inserted. Most of the work was done to test conformal deposition on Si and SiO_2 structures without detailed interest in the interfacial layer.[18–21] Nevertheless, MOCVD is considered to be one of the best techniques for production applications due to its high deposition rates, amenability to large wafer size scaling, and thickness conformability for complex device structures and topographies. However, a serious problem is the control of the amorphous oxide layer between STO thin film and Si substrate.

In this article, we report on the investigation of the microstructure and interfaces of the STO films on silicon (001)-substrates by means of Bragg-diffraction contrast transmission electron microscopy (TEM) and high-resolution transmission electron microscopy (HRTEM). It was found that an amorphous layer occurred at the interfaces. The influence of different MOCVD growth parameters on the film quality and the amorphous interface layer was studied. Especially the influence of the chemical environment on the amorphous layer growth was investigated.

II. EXPERIMENTAL PROCEDURES

The STO thin films were deposited on silicon (001) substrates in a MOCVD system which was described in detail in Ref. 22. In brief, an AIXTRON 2600G3 Planetary Reactor® capable of handling five 6 in. wafers simultaneously was used. The wafers were placed on a coated graphite susceptor carrying five smaller plates. The gas inlet was in the center of the reactor and provided a pure horizontal gas flow direction, making this reactor a radial flow system. A liquid precursor delivery system mixed two different liquid sources: a 0.35 molar solution of $Sr(thd)_2$ and a 0.4 molar solution of $Ti(O{-}iPr)_2(thd)_2$. The liquid mixture was delivered by a micropump to the vaporizer on top of the reactor. Hot argon gas preheated to the evaporation temperature of 235 °C carried the evaporated solution through a quartz nozzle to the substrate. All MOCVD experiments were carried out at a reduced pressure (2 mbar for all films discussed here) in order to increase the gas diffusion and prevent prereactions. The deposition temperature for all the samples was set at 655 °C. The silicon substrates were chemically cleaned and etched by dilute HF acid prior to being inserted into the chamber in order to remove native oxide. Details of the various growth parameters are summarized in Table I.

Both cross-sectional and plan-view specimens were prepared by conventional standard methods. Cross-sectional specimens were prepared by cutting the film-covered wafer into slices. Two of the slices were glued together face to face and embedded in epoxy resin. After the glue was cured, disks with a diameter of 3 mm were obtained by cutting away excess epoxy. These disks were then ground, dimpled, polished, and subsequently Ar-ion milled in a stage cooled with liquid nitrogen. For the plan-view specimens only, substrate sides were thinned by grinding and polishing, followed by dimpling to a thickness of 15 μm and then by ion milling. TEM and HRTEM investigations were carried out in a Philips CM20-FEG electron microscope operated at 200 kV. Compositional homogeneity of the STO thin film was investigated by energy-dispersive x-ray spectroscopy (EDX) using a spot size of about 5 nm.

TABLE I. Deposition conditions for the STO films studied in the present work. The deposition temperature for all the samples was set at 655 °C. The delay time in the third column denotes the starting time of the oxidizer flow. The negative sign denotes the oxidizer admission prior to the film deposition and the positive delay denotes the starting time after the film deposition

Sample	Precursor flow (s)	Oxidizer flow delay/total time (s)	N_2O/O_2 flow rate (sccm)	Thickness of a-SiO_x (nm)
A	440	−60 / 500	0/110	3.8
B	440	0 / 440	0/110	3.8
C	440	30 / 410	0/110	3.7
D	440	120 / 320	0/110	3.7
E	660	0 /660	0/60	3.1
F	440	0 / 440	0/60	3.2
G	220	0 / 220	0/60	3.2
H1	440	−180 / 620	55/55	2.7
H2[a]	440	−180 / 620	55/55	2.8
I	330	0 / 330	55/55	2.6
J	220	0 / 220	55/55	2.7
K	110	0 / 110	55/55	2.1–2.3
L	22	0 / 22	55/55	1.9
M	440	0 / 0		0–1
N	0	0 / 0		0.6
O	0	0 / 700	55/55	0.9
P	0	0 / 700	0/110	1.5
Q	0	0 / 700	0/500	2.2

[a]No HF dip, native oxide layer on Si(100).

III. RESULTS AND DISCUSSION

A. STO thin films

TEM observation of the different samples revealed a similar structural behavior for all of the films. Figure 1 shows a representative cross-sectional low-magnification lattice image of sample B. The image was recorded with the incident electron beam parallel to the [110] zone axis of the silicon substrate. We see from the image that the STO thin film, which is about 20 nm thick, has a polycrystalline structure. An amorphous layer evidently exists between the film and the substrate. The interface between the crystalline film

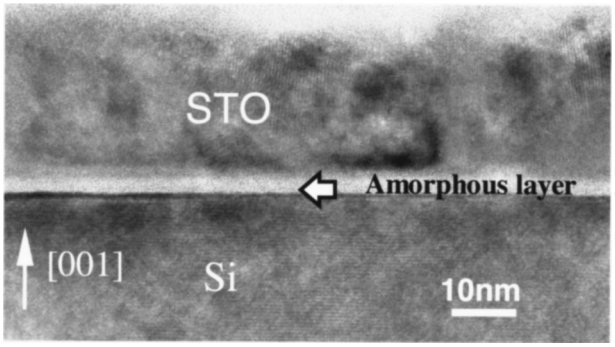

FIG. 1. Cross-sectional low-magnification lattice image of sample B: an amorphous interfacial layer and a polycrystalline STO film is observed on the silicon (001) substrate.

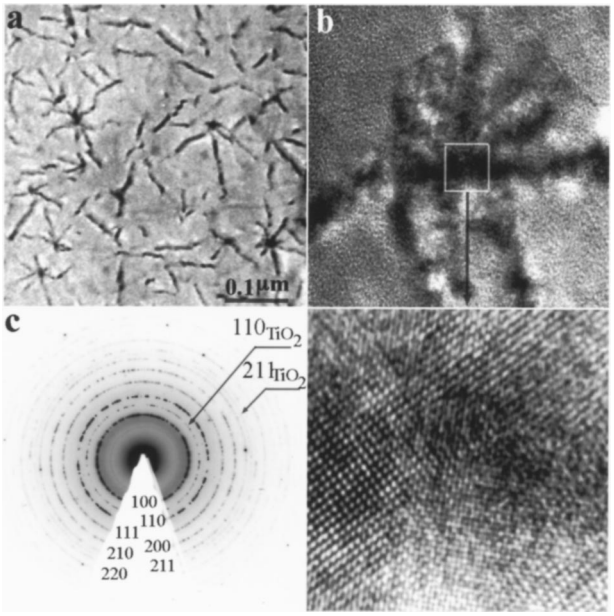

FIG. 2. (a) Diffraction contrast image taken from a plan-view specimen of the sample H2; (b) lattice image of a claw-like dark region in (a); (c) SAED pattern showing polycrystalline diffraction rings, which can be fully indexed as reflections of the STO and TiO_2 crystals.

and the amorphous layer looks flat. Figure 2(a) displays a plan-view Bragg-diffraction contrast micrograph of sample H2. From cross-sectional and plan-view images a grain size of 10–20 nm was measured within the film plane, which also corresponds to the film thickness of about 20 nm. We can also see a feature of claw-like dark contrast distributed in the film. HRTEM investigation showed that this claw-like contrast corresponds to the grains which show a low index zone axis parallel to the film normal. In many cases, the zone axis is ⟨001⟩. A lattice image of this area is shown in Fig. 2(b) with two different magnifications. Figure 2(c) shows a selected-area electron diffraction pattern with many rings, which is typical of the polycrystalline film. All of the allowed reflections for the STO crystal can be found in this ring pattern, indicating that the grains in the film are randomly oriented. In addition, we also find two extra diffraction rings which can be indexed as belonging to TiO_2. EDX spectroscopy analysis of small areas (about 5 nm in diameter) was performed for different areas of the plan-view samples. We found that the chemical composition of the film is inhomogeneous. Interestingly, in the well-oriented grains, i.e., the claw-like dark regions in the low magnification image of Fig. 2(a), a Sr/Ti atomic ratio of 1.0 was measured, while in the other regions a lower Sr/Ti atomic ratio of 0.93 was obtained. On average the film is Ti rich, which is in good agreement with the results of x-ray fluorescence (XRF) analysis (Sr/Ti=0.94). Hence, although the film is on average Ti rich, the STO grains show an ideal stoichiometry and the extra Ti is believed to be concentrated in the TiO_2 grains detected by the diffraction analysis.

A similar behavior was also observed for other films grown with a sufficient amount of oxidizer, even if the average composition of the deposited film stack as determined by XRF was slightly Sr rich. This precipitation of TiO_2 in the crystalline surface layer is consistent with the observation of a higher Ti concentration in this region due to stronger Sr interdiffusion into the interface region, which is discussed below (Fig. 8). Only for the case of sample M did we observe significant changes in the microstructure: there is a drastically reduced grain size (perpendicular to the film surface) and an appreciable amount of carbon in the film, as discussed below.

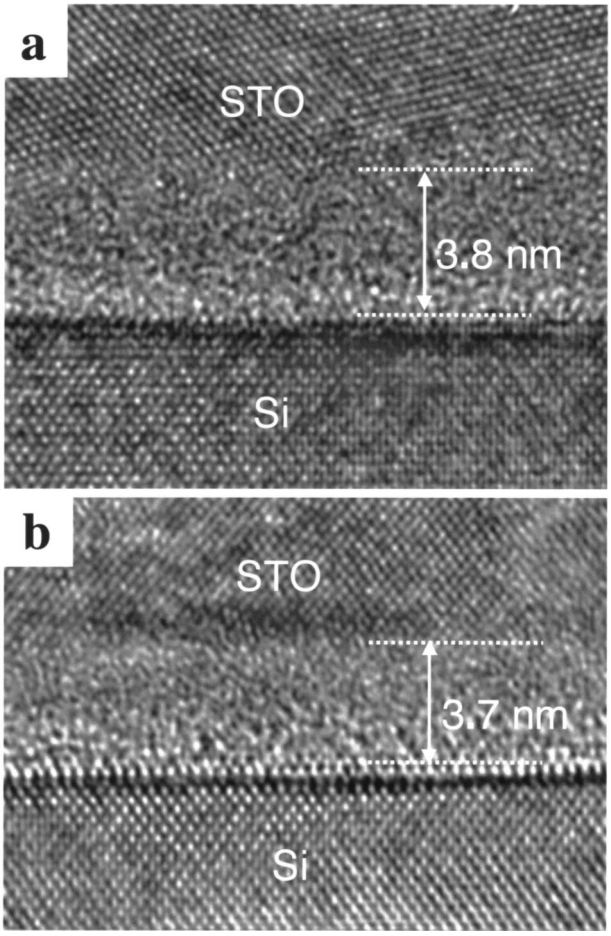

FIG. 3. Cross-sectional lattice images of two different STO films. (a) Sample A prepared with admission of oxygen for 60 s prior to the film deposition; (b) Sample D prepared with admission of oxygen 120 s after the start of the precursor inlet. The other deposition parameters were the same.

B. Observation of amorphous interfacial layers

HRTEM observation of the cross-sectional specimens showed evidence for the existence of an amorphous interfacial layer between the STO film and the Si substrate for all samples as summarized in Table I. The thickness of the amorphous layer depended on the growth conditions. According to the range of the layer thickness we classify the samples into four groups: the first three groups, A–D , E–G, and H–L were grown with oxidizer flow values which yielded perfectly (100) textured $(Ba_xSr_{1-x})TiO_3$[22] and STO films on Pt(111) substrates; only the last run, M, had a minimum oxidizer flow determined by the precursor itself.

For the first group, samples A, B, C, and D, which were grown with the highest oxidizer flow, the amorphous layer has a thickness of about 3.7 nm. Figures 3(a) and 3(b) show

the cross-sectional micrographs of sample A and sample D, respectively, taken with the incident electron beam parallel to the [110]-axis zone of silicon substrate. The difference in growth conditions of these four samples is only the oxygen-flow time, as shown in Table I. The other parameters are the same. The oxygen-flow time is the longest for sample A (500 s, oxygen started to flow 60 s prior to deposition), and the shortest for sample D (320 s, oxygen started to flow after 120 s of deposition). The fact that no evident difference in the thickness of the amorphous layers is detected in these four samples indicates that no effective diffusion barrier can be formed in the initial state of deposition and the formation of the amorphous layer cannot be suppressed in this way.

In order to investigate the influence of the oxygen in more detail the second series (samples E–G) was run with about half of the oxidizer flow. As the total pressure in the reactor was constant, this reduced flow corresponds to about half of the oxygen partial pressure during deposition. We observe a decrease of the layer thickness to an average value of 3.2 nm. In addition, the deposition time was varied by a factor of three without a significant change of the thickness of the amorphous layer. Hence, some saturation value might be reached after a short time for the given partial pressures of precursor and oxygen.

For the third series, H–L, the oxidizer was modified, i.e., the oxygen flow was nearly the same as for group 2, but the same amount of N_2O was added. We observed a further decrease of the amorphous layer thickness to about 2.7 nm for a precursor run time of 440 s, which also corresponds to the saturation value. Within this series, we tested in addition the influence of surface cleaning before deposition. Sample H1 was chemically cleaned and etched by dilute HF acid prior to deposition and for sample H2 the native oxide layer was not removed. STO films were simultaneously deposited in one run and the corresponding lattice image is shown in Figs. 4(a) and 4(b), respectively, and an amorphous interfacial layer with a thickness of about 2.7 nm is observed for both samples (Table I). The surface treatment seems to have no visible effect on the thickness of the amorphous layer for the given total thickness. In addition very short deposition runs were included, which show a fast initial growth of the amorphous layer.

The fourth group, which includes sample M only, was prepared under special conditions, i.e., no oxygen was supplied into the growth atmosphere. Figure 5 shows the cross-sectional lattice images taken from different interface areas of sample M. In Fig. 5(a) the thickness of the amorphous layer is measured approximately as 1.0 nm. In Fig. 5(b) the amorphous layer is hardly seen and a direct contact of the film to the silicon substrate is evident. Hence, on average this sample shows the thinnest amorphous interfacial layer (<1.0 nm).

Finally, some test runs were performed with samples N–Q. The starting point of the growth of the amorphous film is the flow time of the precursors into the reactor. However, it must be taken into account that after HF dipping the samples were transferred to the reactor, which was subsequently evacuated to the minimum pressure of the reactor of 0.2 mbar, heated to 655 °C, and temperature stabilized.

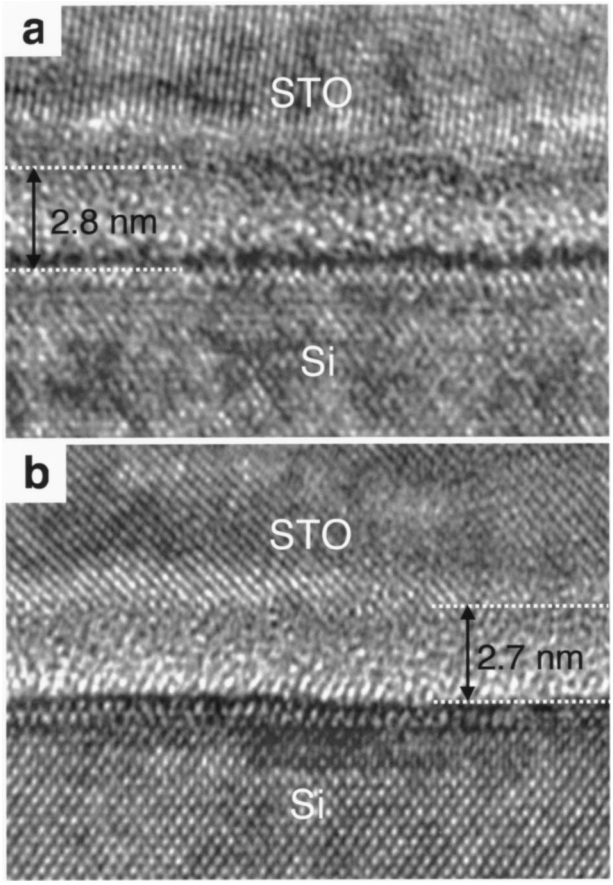

FIG. 4. Cross-sectional lattice images of STO films grown on differently prepared Si(001) substrates. (a) sample H1: the surface of the silicon substrate was HF dipped prior to film deposition; (b) sample H2: the surface of the silicon substrate was not dipped before deposition.

Sample N corresponds to this starting position, which typically corresponds to about 2500 s at 655 °C, and we already observed a SiO_x thickness of 0.6 nm, which can therefore be regarded as a minimum thickness. Increasing the oxidizer partial pressure after this stabilization period at 655 °C to a flow rate of 55/55 sccm yields only small further growth to a thickness of 0.9 nm (sample O). An increase to the maximum oxygen flow of 110 sccm used for depositions resulted in a layer thickness of 1.5 nm (sample P) and represents the maximum value expected for thermal growth under the present conditions. A further increase to 500 sccm yields an increase of the layer thickness to 2.2 nm and gives additional evidence for the relevance of this growth parameter.

C. Discussion of the growth of the amorphous interlayer

Figure 6 summarizes the observed thickness of the amorphous layer after different deposition times in different oxidizer atmospheres. The dependence of the layer thickness on the oxidizer flow rate is additionally summarized in Fig. 7 for films with a precursor flow time of 440 s. The growth rates for thermal oxidation are included in Fig. 7 for comparison to the growth rates under deposition conditions. Much larger growth rates are observed when the deposition occurs. Due to this difference the additional oxidation time

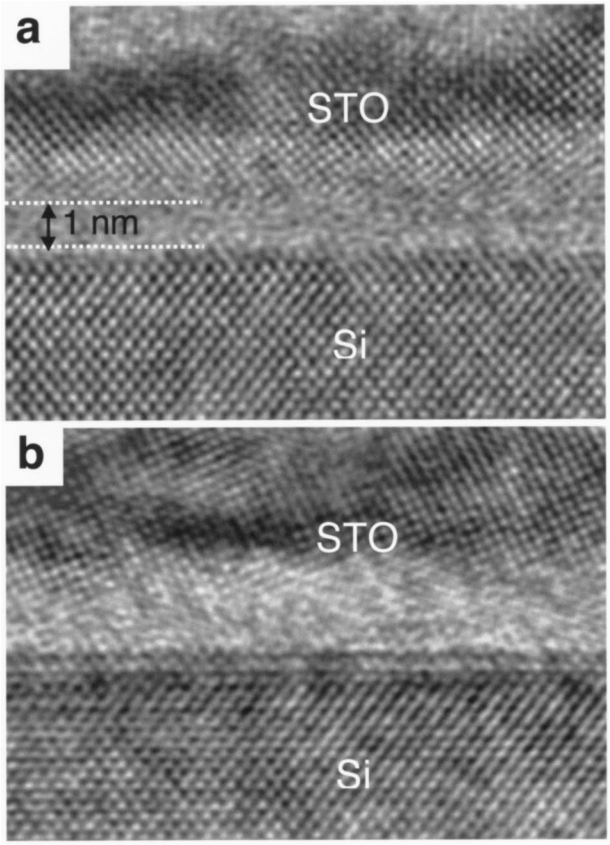

FIG. 5. Cross-sectional lattice images of sample M, taken from different areas: (a) an interface area including an amorphous layer with a thickness of 1.0 nm; (b) an interface area without visible amorphous layer.

under the oxidizer for samples A and H does not seem to be relevant and is not considered in Fig. 6. The absolute values of the thermal oxide growth rates correspond to the very fast initial growth step as discussed in detail by Gusev *et al.*[23] and are therefore not comparable to detailed growth models (e.g., Deal and Grove[24]) which rely on data gathered at much higher temperatures ($>700\,^{\circ}$C). Nevertheless, Fig. 7 reveals a strong dependence of the layer thickness on the oxygen partial pressure.

Most important, however, is the increase of the growth rate in the presence of the precursors. For these conditions

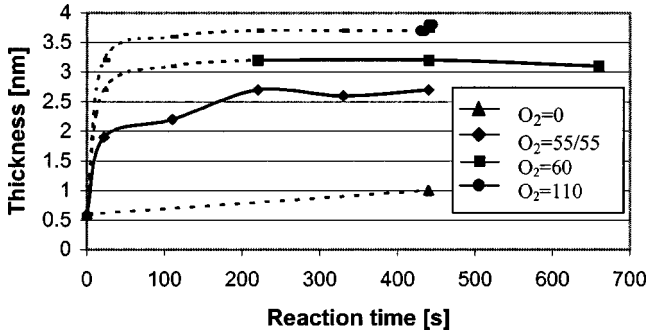

FIG. 6. Thickness of the amorphous layer vs deposition time (precursor run time) for different oxidizers as specified in the inset. The starting value of 0.6 nm is grown during the heating and thermal stabilization of the substrate at 655 °C. Dashed lines are a guide for the eye only.

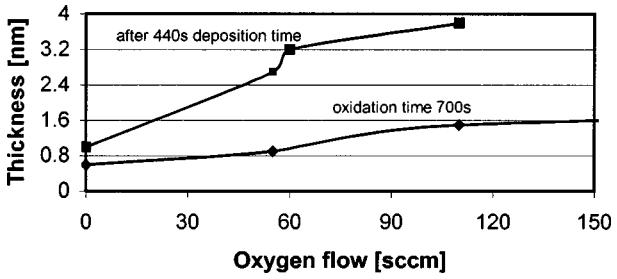

FIG. 7. Thickness of the amorphous layer vs oxygen flow rate for a deposition time of 440 s, which yields a "saturation thickness" as shown in Fig. 6. The value at 55 sccm seems reduced due to the addition of 55 sccm N_2O. Thermal oxidation rates after 700 s for the same oxygen flow are included for comparison.

the kinetics has been investigated in some more detail and Fig. 6 shows a fast initial growth and a quasisaturation region. Such behavior can be explained by initially kinetically controlled growth and a transition to slow diffusion-limited growth as soon as there is a sufficiently thick closed film. Similar kinetics have been observed by Ramdani *et al.*[9] for epitaxial film growth of STO on Si(100). This observation of increased layer growth as compared to thermal oxidation is comparable to the increased reaction rate for Y_2O_3 layers,[25,26] which was attributed to catalytic effects and/or complex reaction paths. The importance of the details of the reaction paths is further stressed by the observation of the reduction of the growth rate by the addition of N_2O (compare 60 sccm O_2 with 55 sccm O_2 + 55 sccm N_2O, Fig. 6). This reduction due to the admission of an additional oxidizer might not only be due to the release of oxygen from N_2O but also to the reaction of the atomic oxygen with N_2O forming 2NO and/or NO_2 (for details see Ref. 27). Hence, an appropriate choice of oxidizer might help to suppress the growth of the amorphous interlayer.

Using the precursor without additional oxidizer we succeeded in reducing the amorphous layer thickness dramatically; at some places there actually seems to be direct crystal contact with the Si substrate. Hence the layer thickness may be reduced to a level which is acceptable for application as a gate oxide. However, incomplete precursor reactions and a related dramatic increase of the carbon content of the films is revealed by secondary neutral-atom mass spectrometry (SNMS), see Fig. 8, for these conditions. In addition a strong interdiffusion, which is much more serious for Sr than for Ti, is observed in Fig. 8. Hence, the interfacial layer is not pure SiO_2, and SrO_x and/or silicates must be considered and further investigated. This observation of a strong interdiffusion is further supported by the comparison of the TEM results, localized on the STO layer, with XRF results which average the whole stack: XRF yields quite generally a larger layer thickness of STO and a higher Sr content. Such discrepancies are not observed for STO films deposited on Pt electrodes.

IV. SUMMARY AND CONCLUSION

The microstructure and interfaces in thin films of STO deposited by MOCVD on Si(001) substrates were studied by TEM and HRTEM. We find that the main factor dominating

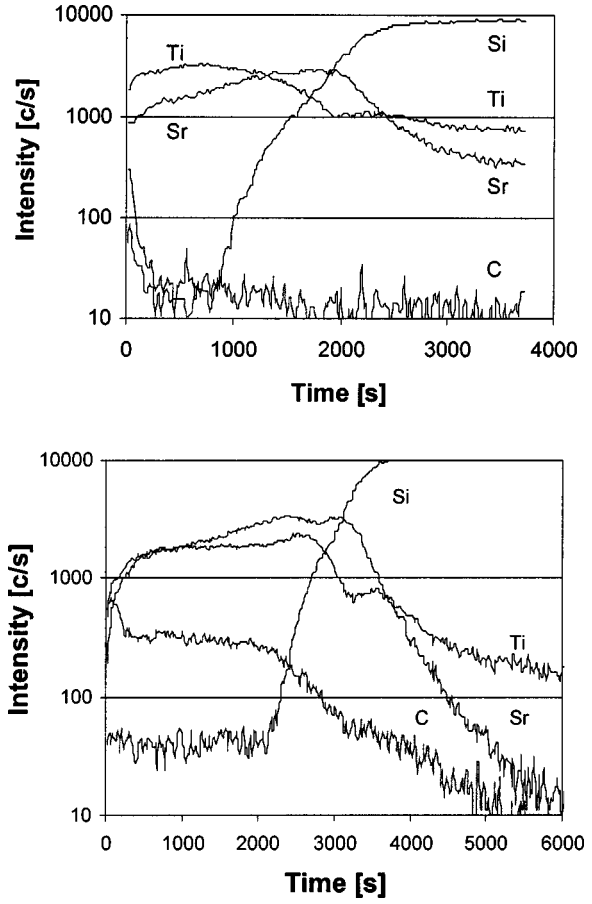

FIG. 8. SNMS of samples H1 and M showing similar interdiffusion and a dramatic increase of the carbon content with reduction of oxidizer flow.

the thickness of the amorphous layer between the Si(001) substrate and the STO thin film is the oxygen partial pressure used in the film growth. The results can be summarized as follows:

(a) Films deposited under sufficient oxidizer partial pressure consist of randomly oriented grains with a grain size in the range of 10–20 nm. This polycrystalline growth occurs as a result of an amorphous SiO_x layer that is already present at the beginning of the deposition. Hence, differently oriented STO islands nucleate, grow, and finally coalesce to a continuous polycrystalline film. For Ti-rich films, the excess Ti exists in the form of TiO_2 precipitates, while the individual STO grains show a stoichiometric chemical composition within the experimental uncertainty. However, for a very low oxidizer supply carbon-rich films with even smaller grain sizes and amorphous regions are observed.

(b) HRTEM images reveal an amorphous layer at the interface between the films and the substrates. The interfacial layer thickness showed a rapid initial increase, which is much faster than thermal SiO_2 growth under the same oxygen pressure, and approaches a saturation value within the given experimental uncertainties. Consistent with this saturation behavior, a short-time preadmission or delay of oxygen admission relative to the precursor admission shows no visible effect on the average thickness of the amorphous layer when the other parameters remain unchanged. Such a behavior corresponds to a fast reaction-limited step and a transition to a slow diffusion-limited growth regime.

(c) The thickness of the interfacial layer increases with the oxygen partial pressure present during film deposition. Mixing of N_2O with oxygen reduces the thickness of the amorphous layer and indicates an interesting possibility of reducing the growth of the amorphous layer by modifying the oxidizer chemistry and the details of the reaction paths. In addition, this growth might be influenced by the interdiffusion of Ti and especially of Sr. A dramatic reduction to a value acceptable for gate-oxide applications was achieved by lowering the oxidizer pressure to the minimum value given by the oxygen content of the present precursors. However, this comes at the cost of a dramatic increase in the carbon content of the film.

[1] S. R. Summerfelt, in *Thin Film Ferroelectric Materials and Devices*, edited by R. Ramesh (Kluwer, Boston, MA 1997), pp. 1–42.
[2] G. D. Wilk, R. M. Wallace, and J. M. Anthony, J. Appl. Phys. **89**, 5243 (2001).
[3] D. G. Schlom and J. H. Haeni, MRS Bull. **27**, 198 (2002), and references therein.
[4] B. K. Moon and H. Ishiwara, Jpn. J. Appl. Phys., Part 1 **33**, 1472 (1994).
[5] H. Mori and H. Ishiwara, Jpn. J. Appl. Phys., Part 2 **30**, L1415 (1991).
[6] T. Tambo, T. Nakamura, K. Maeda, H. Ueba, and C. Tatsuyama, Jpn. J. Appl. Phys., Part 1 **37**, 4454 (1998).
[7] R. A. McKee, F. J. Walker, and M. F. Chisholm, Phys. Rev. Lett. **81**, 3014 (1998).
[8] R. A. McKee, F. J. Walker, and M. F. Chisholm, Nature (London) **293**, 468 (2001).
[9] J. Ramdani, R. Droopad, Z. Yu, J. A. Curless, C. D. Overgaard, J. Finder, K. Eisenbeiser, J. A. Hallmark, W. J. Ooms, V. Kaushik, and P. Alluri, Appl. Surf. Sci. **159-160**, 127 (2000).
[10] K. Eisenbeiser, J. M. Finder, Z. Yu, J. A. Curless, J. A. Hallmark, R. Droopad, W. J. Ooms, L. Salem, S. Bradshaw, and C. D. Overgaard, Appl. Phys. Lett. **76**, 1324 (2000).
[11] K. Droopad, Z. Yu, J. Ramdani, L. Hilt, J. Curless, C. Overgaard, J. L. Edwards, J. Finder, K. Eisenbeiser, J. Wang, V. Kaushik, B.-Y. Ngyuen, and B. Ooms, J. Cryst. Growth **227-228**, 936 (2001).
[12] O. Nakagawara, M. Kobayashi, Y. Yoshino, Y. Katayama, H. Tabata, and T. Kawai, J. Appl. Phys. **78**, 7226 (1995).
[13] S. Migita and S. Sakai, J. Appl. Phys. **89**, 5421 (2001).
[14] R. D. Vispute, J. Narayan, K. Dovidenko, K. Jagannadham, N. Parikh, A. Suvkhanov, and J. D. Budai, J. Appl. Phys. **80**, 6720 (1996).
[15] C. Wang, V. Kugler, U. Helmersson, N. Konofao, E. K. Evangelou, S. Nakao, and P. Jin, Appl. Phys. Lett. **79**, 1513 (2001).
[16] L. Mechin, G. J. Gerritsma, and J. Gracia Lopez, Physica C **324**, 47 (1999).
[17] S. H. Nam, W. J. Lee, and H. G. Kim, J. Phys. D **27**, 866 (1994).
[18] H. Yamaguchi, P. Lesaicherre, T. Sakuma, Y. Miyasaka, A. Ishitani, and M. Yoshida, Jpn. J. Appl. Phys., Part 1 **32**, 4069 (1993).
[19] K. Frohlich, D. Machajdik, A. Rosova, I. Vavra, F. Weiss, B. Bochu, and J. P. Senateur, Thin Solid Films **260**, 187 (1995).
[20] S. Y. Park, J. Choi, and K. No, Jpn. J. Appl. Phys., Part 1 **40**, 2456 (2001).
[21] W. Ma, P. Schäfer, P. Ehrhart, and R. Waser, Integr. Ferroelectr. **30**, 139 (2000).
[22] P. Ehrhart, F. Fitsilis, S. Regnery, R. Waser, F. Schienle, M. Schumacher, M. Dauelsberg, P. Strzyzewski, and H. Juergensen, Integr. Ferroelectr. **30**, 183 (2000).
[23] E. P. Gusev, H. C. Lu, T. Gustafsson, and E. Garfunkel, Phys. Rev. B **52**, 1759 (1995).
[24] R. E. Deal and A. S. Grove, J. Appl. Phys. **36**, 3770 (1965).
[25] V. Misra, G. Lucovsky, and G. Parsons, MRS Bull. **27**, 212 (2002).
[26] J. J. Chambers and G. N. Parsons, J. Appl. Phys. **90**, 918 (2001).
[27] S. Singhvi and C. G. Takoudis, J. Appl. Phys. **82**, 442 (1997).